The Parameter Planes of the Spherically Symmetric and Static Relativistic Solutions for Polytropes

Jorge L. deLyra*

Universidade de São Paulo
Instituto de Física
Rua do Matão, 1371,
05508-090 São Paulo, SP, Brazil

April 21, 2023

Abstract

We explore the parameter space of the family of static and spherically symmetric solutions of the Einstein field equations for polytropes, that were presented in a previous paper. This is four-parameter family of exact solutions, of which one parameter can be factored out, so that there are only three essential free parameters. The solutions are exact in the sense that no approximations are involved, other than those implied by the numerical precision limitations. The primary objective of this exploration is to establish the existence of large collections of specific solutions, and to determine their main properties.

For each value of one of the three essential free parameters of the family of solutions, the polytropic index n, taken here, for simplicity's sake, to be either an integer or a half-integer, we define and explore the parameter planes spanned by the other two essential free parameters. In this way, besides establishing their existence, as are also able to classify the solutions according to their overall matter energy density, as well as in terms of their proximity to solutions that display an event horizon.

For four values of n we successfully establish an allowed region of the parameter planes, where the solutions not only exist but also correspond to physically acceptable matter. We find that there are solutions within these regions with overall matter energy densities varying all the way from very low to very high, including some that are as close as one may wish to solutions that display an event horizon, and that therefore represent black holes, or extremely dense objects very similar to them.

Keywords:
General Relativity, Einstein Equations, Solutions for Polytropes.

DOI: 10.5281/zenodo.XXXXXXX

*Email: delyra@lmail.if.usp.br ORCID: 0000-0002-8551-9711

1 Introduction

In a previous paper [1] we established the solution of the Einstein field equations for the case of spherically symmetric shells of gaseous fluid located between radial positions r_1 and r_2 of the Schwarzschild system of coordinates. These solutions are exact in the sense that they involve no approximations, but they are not written entirely in closed analytical form. While all relevant functions describing both the geometry and the matter are written analytically in terms of a single function, which we denote by $\beta(r)$, and although the main properties of this function can also be established analytically, it is still necessary to determine this function in detail by numerical means, including the existence of the internal and external radii r_1 and r_2, and therefore the existence of the solution itself.

In this paper we will present a fairly extensive numerical exploration of the parameter space of these solutions, in order to establish the general picture in regards to their existence and to their main properties. Connections with some special cases which are already well known will be pointed out. Some diagnostic observables will be defined and calculated, which were designed to put in evidence some of the most important properties of the solutions. In this paper we will be limited to the case in which the polytropic index n, which is one of the free parameters, is *strictly* larger that 1, that is, satisfies $n > 1$.

This paper is organized as follows: in Section 2 we quickly review the new class of static and time-independent exact solutions for gaseous shells; in Section 3 we discuss the parameter planes for each value of the polytropic index n, and examine in particular the allowed regions in each case; in Section 4 we discuss the definition and the behavior of the diagnostic observables over the allowed regions; in Section 5 we discuss in general terms how to apply the solutions to problems in astrophysics; and in Section 6 we state our conclusions.

2 Review of the Polytropic Solutions

In this section we will quickly review the solutions for gaseous fluids presented in [1], in order to establish the notation, as well as the basic character of the solutions. Both the notation and the ideas presented in [1] rely on some of the notation and ideas presented in the previous paper [2], in which we presented the exact solution for the case of liquid fluids. In this work we will use the time-like signature $(+,-,-,-)$, following [3]. In terms of the coefficients of the metric, for an invariant interval given in terms of the Schwarzschild coordinates (t, r, θ, ϕ) by

$$ds^2 = \mathrm{e}^{2\nu(r)}c^2dt^2 - \mathrm{e}^{2\lambda(r)}dr^2 - r^2\left[d\theta^2 + \sin^2(\theta)d\phi^2\right], \tag{1}$$

where $\exp[\nu(r)]$ and $\exp[\lambda(r)]$ are two positive functions of only r, as was explained in [2] the Einstein field equations reduce to the set of three first-order differential equations

$$\left\{1 - 2\left[r\lambda'(r)\right]\right\}\mathrm{e}^{-2\lambda(r)} = 1 - \kappa r^2\rho(r), \tag{2}$$

$$\left\{1 + 2\left[r\nu'(r)\right]\right\}\mathrm{e}^{-2\lambda(r)} = 1 + \kappa r^2 P(r), \tag{3}$$

$$\left[\rho(r) + P(r)\right]\nu'(r) = -P'(r), \tag{4}$$

where $\rho(r)$ is the energy density of the matter, $P(r)$ is its isotropic pressure, and the constant κ is given by $\kappa = 8\pi G/c^4$, where G is the universal gravitational constant and c is the speed of light. In these equations the primes indicate differentiation with respect to r.

It is convenient for the analysis of the solutions to change variables in the field equations from the function $\lambda(r)$ to a function $\beta(r)$, which is defined to be such that

$$\mathrm{e}^{2\lambda(r)} = \frac{r}{r - r_M \beta(r)}, \tag{5}$$

where $r_M = 2GM/c^2$ is the Schwarzschild radius associated to the total asymptotic gravitational mass M, which then implies that we have for the corresponding derivatives

$$2r\lambda'(r) = -r_M \, \frac{\beta(r) - r\beta'(r)}{r - r_M \beta(r)}. \tag{6}$$

Note that $\beta(r) = 0$ corresponds to $\lambda(r) = 0$ and therefore to $\exp[2\lambda(r)] = 1$ for the radial coefficient of the metric. In such cases the variations of the radial coordinate are equal to the variations of the corresponding proper radial length. Substituting the expressions in Equations (5) and (6) in the component field equation shown in Equation (2) a very simple relation giving the derivative of $\beta(r)$ in terms of $\rho(r)$ results,

$$\beta'(r) = \frac{\kappa r^2 \rho(r)}{r_M}. \tag{7}$$

Therefore, in any interval where $\rho(r) = 0$ we have that $\beta(r)$ is a constant. Since we must have that $\rho(r) \geq 0$, it therefore follows that $\beta(r)$ is a monotonically increasing function, which is a constant if and only if we are within a vacuum region. In addition to this, since according to the asymptotic boundary condition we must have that $\beta(r) \to 1$ when $r \to \infty$, it also follows that $\beta(r)$ is limited from above by 1. Note that these facts are completely general for the spherically symmetric static case, irrespective of the type of fluid matter which is present within the matter region.

In the previous paper [1] we established the solution of the Einstein field equations for the case of a spherically symmetric shell of gaseous fluid located between the radial positions r_1 and r_2 of the Schwarzschild system of coordinates. These positions are *not* arbitrary, but rather are obtained as part of the solution of the problem. For this problem we assume the hypothesis that the gas satisfies the polytropic equation of state

$$P(r) = K \left[\rho(r)\right]^{1+1/n}, \tag{8}$$

where K, the polytropic constant, is a positive constant, and $n > 1$, the polytropic index, is a real number that, merely for simplicity, may be taken to be an integer or half-integer. For convenience we define the auxiliary quantity

$$F(r) = K \left[\rho(r)\right]^{1/n}, \tag{9}$$

in terms of which the equation of state becomes simply

$$P(r) = F(r)\rho(r). \tag{10}$$

As was shown in [1], given the field Equations (2) through (4) and the equation of state shown in Equation (8), the solution for $\lambda(r)$ is given by

$$\lambda(r) \;=\; \begin{cases} -\dfrac{1}{2}\,\ln\!\left(\dfrac{r + r_\mu}{r}\right) & \text{for} \quad 0 < r \leq r_1, \\[2ex] -\dfrac{1}{2}\,\ln\!\left[\dfrac{r - r_M\beta(r)}{r}\right] & \text{for} \quad r_1 \leq r \leq r_2, \\[2ex] -\dfrac{1}{2}\,\ln\!\left(\dfrac{r - r_M}{r}\right) & \text{for} \quad r_2 \leq r < \infty, \end{cases} \tag{11}$$

where once more $r_M = 2GM/c^2$, while for $\nu(r)$ we have

$$\nu(r) = \begin{cases} \frac{1}{2}\ln\left(\frac{1-r_M/r_2}{1+r_\mu/r_1}\right) + \frac{1}{2}\ln\left(\frac{r+r_\mu}{r}\right) & \text{for} \quad 0 < r \leq r_1, \\ \nu(r_2) - (n+1)\ln[1+F(r)] & \text{for} \quad r_1 \leq r \leq r_2, \\ \frac{1}{2}\ln\left(\frac{r-r_M}{r}\right) & \text{for} \quad r_2 \leq r < \infty. \end{cases} \tag{12}$$

The solution introduces into the system, through the interface boundary conditions, the new physical parameter r_μ with dimensions of length, which can be associated to a mass parameter μ in the same way that r_M is associated to M, namely by $r_\mu = 2G\mu/c^2$. As was also shown in [1], the determination of the function $\beta(r)$ in the matter region leads with no further difficulty to the determination of all the functions that describe both the matter and the geometry of the system, by means of the exact analytical relations

$$\rho(r) = \frac{r_M \beta'(r)}{\kappa r^2}, \tag{13}$$

$$P(r) = K\left[\frac{r_M \beta'(r)}{\kappa r^2}\right]^{1+1/n}, \tag{14}$$

$$F(r) = K\left[\frac{r_M \beta'(r)}{\kappa r^2}\right]^{1/n}, \tag{15}$$

$$\lambda(r) = \frac{1}{2}\ln\left[\frac{r}{r - r_M\beta(r)}\right], \tag{16}$$

$$\nu(r) = \nu(r_2) - (n+1)\ln[1+F(r)]. \tag{17}$$

The four free parameters of the system are K, n and M, all of which describe the nature and state of the matter, and the value of $\beta'(r)$ at its point of maximum, which can also be seen to be related to the matter, since it determines the general scale of the matter energy density, as can be seen from Equation (7). Note that the radial positions r_1 and r_2 are not chosen by hand, and are defined as the positions where the matter energy density $\rho(r)$ becomes zero. As was shown in [1], this differential system has the property that once $\rho(r)$ hits the value zero during the integration, in either direction, it stays at zero from that point on, thus generating a vacuum region.

For all sets of parameters for which there is a solution of the differential problem the function $\beta'(r)$ has a single point of maximum within the matter region, which is the point where $\beta(r)$ has its single inflection point. As was also shown in [1], for all existing solutions with $r_1 > 0$ it holds that $r_\mu > 0$. This strictly positive value of r_μ implies that the solutions have singularities at the origin. However, that type of singularity is not associated to an infinite concentration of matter, but rather, as explained in [2], to exactly zero matter energy density at that point.

Both for the subsequent analysis and for the numerical approach, it is convenient to further transform variables at this point, in order to write everything in terms of dimensionless variables and functions. In order to do this we must now introduce an arbitrary radial reference position $r_0 > 0$. For now the value of this parameter remains completely arbitrary, other than that it must be strictly positive, and has no particular physical meaning. It is only a mathematical device that allows us to define a dimensionless radial variable and a dimensionless parameter associated to the mass M by

$$\xi = \frac{r}{r_0}, \tag{18}$$

$$\xi_M = \frac{r_M}{r_0}, \tag{19}$$

as well as to define the dimensionless function of ξ, to assume the role of $\beta(r)$,

$$\gamma(\xi) = \xi_M \beta(r). \tag{20}$$

Note that the asymptotic condition that $\beta(r) \to 1$ for sufficiently large r translates here as the condition that $\gamma(\xi) \to \xi_M$ for sufficiently large ξ. Note also that, since $\beta(r)$ is a limited monotonic function, it follows from Equation (20) that similar conclusions can be drawn for $\gamma(\xi)$, which is therefore a monotonically increasing function which is limited from above, the upper limit in this case being the parameter ξ_M. We also have that $\gamma(\xi)$ is constant within vacuum regions. As was shown in [1] the function $\gamma(\xi)$, and thus the function $\beta(r)$ as well, are both determined by the second-order ordinary differential equation

$$\pi'(\xi) = \pi(\xi) \left\{ \frac{2}{\xi} - \frac{n}{n+1} \frac{1}{\xi - \gamma(\xi)} \frac{1 + F(\xi,\pi)}{2F(\xi,\pi)} \left[\frac{\gamma(\xi)}{\xi} + F(\xi,\pi)\pi(\xi) \right] \right\}, \tag{21}$$

where $\pi(\xi) = \gamma'(\xi)$ is the derivative of $\gamma(\xi)$, the primes now indicate derivatives with respect to ξ, and $F(\xi,\pi)$ is given by

$$F(\xi,\pi) = C \left[\frac{\pi(\xi)}{\xi^2} \right]^{1/n}, \tag{22}$$

where $C = K/\left(\kappa r_0^2\right)^{1/n}$ is a dimensionless constant associated to the polytropic constant K. This differential system can be interpreted either as a second-order ordinary differential equation for $\gamma(\xi)$, or as one of a pair of first-order coupled ordinary differential equations determining $\gamma(\xi)$ and $\pi(\xi)$, the other equation being simply

$$\gamma'(\xi) = \pi(\xi). \tag{23}$$

This second interpretation is the one we adopted in [1], and we will also adopt it here. This pair of first-order ordinary differential equations can be used for the numerical integration of this differential system, in order to obtain $\gamma(\xi)$ and $\beta(r)$, as we in fact did in that paper, and as we will do here as well. It is important to note that in terms of these dimensionless variables the equation of state shown in Equation (8) can be written as

$$\bar{P}(\xi) = C \left[\bar{\rho}(\xi)\right]^{1+1/n}, \tag{24}$$

where we defined the dimensionless pressure and energy density by

$$\bar{P}(\xi) = \kappa r_0^2 P(\xi), \tag{25}$$

$$\bar{\rho}(\xi) = \kappa r_0^2 \rho(\xi). \tag{26}$$

We also have for the relation in Equation (7), when written in terms of the dimensionless variables,

$$\pi(\xi) = \xi^2 \bar{\rho}(\xi). \tag{27}$$

Note that in this formulation of the problem all dimensionfull physical quantities have vanished from view, and the problem is reduced to purely mathematical terms. All that is involved is a dimensionless function $\gamma(\xi)$ of a dimensionless variable ξ, its derivative $\pi(\xi)$,

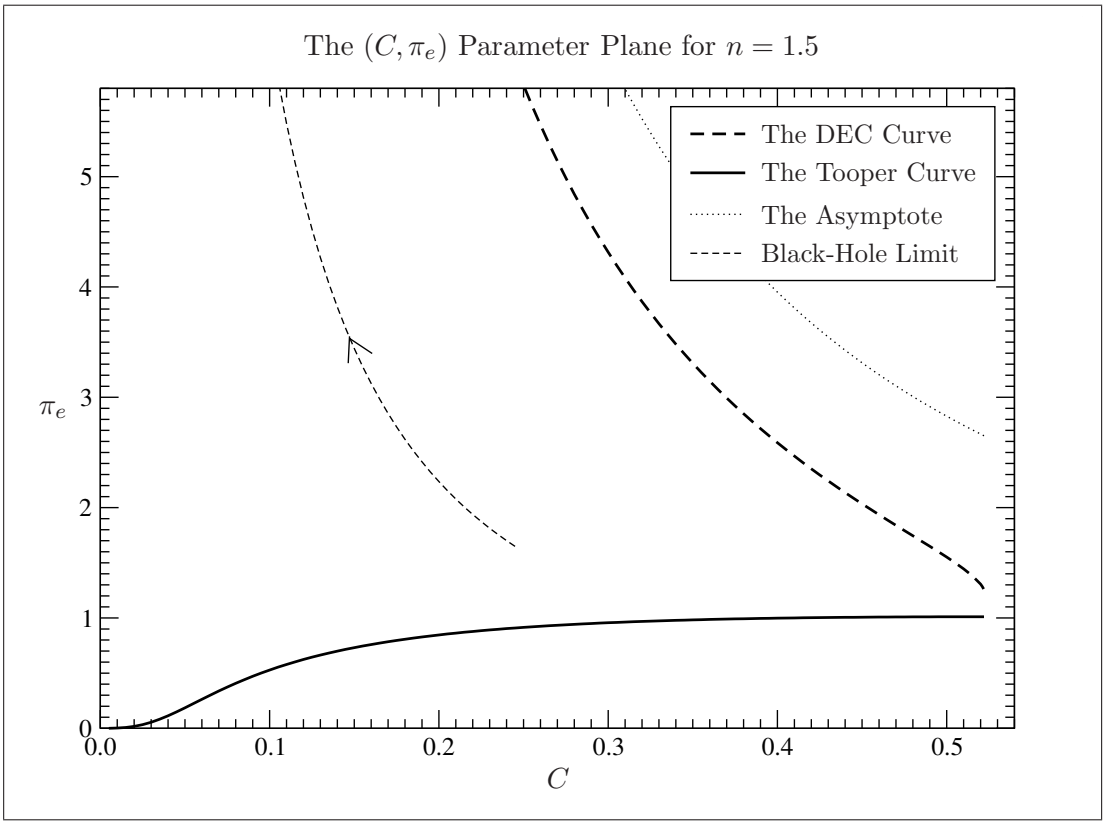

Figure 1: The (C, π_e) parameter plane for the case $n = 1.5$. The Tooper curve approaches the origin as an integer power, namely as C^3. The asymptote is given by $\pi_e = 1/C^{1.5}$.

and two dimensionless positive real constants, n and C. In particular, the mass M and the Schwarzschild radius r_M no longer appear explicitly in the equations. In essence they have been replaced by the parameters r_0 and ξ_M, where this last one appears only as the asymptotic limit of $\gamma(\xi)$. This is a free parameter of the system that has effectively been factored out of it. Later on, in Section (5), we will see that what this means is that there are solutions for all possible values of M and r_M. A careful and complete mathematical study of this dimensionless differential system, followed by a complete tabulation of all the properties of $\gamma(\xi)$, is all that stands between our current semi-analytical solution of the problem and what one could describe as a completely analytical solution of that problem. Some of the relevant properties of $\gamma(\xi)$ were in fact derived in [1].

3 The Parameter Planes

We will begin by simply presenting the results of an extensive numerical exploration of the solutions, and subsequently we will discuss each element that was involved in this exploration. In their dimensionless formulation, the solutions are described by the three dimensionless free parameters n, C and $\pi_e = \pi(\xi_e)$, where ξ_e is the position of the inflection point of $\gamma(\xi)$, which is also the position of the maximum π_e of $\pi(\xi)$. For each value of n, the solutions can be classified according to a parameter plane spanned by C and π_e. In this paper we will limit ourselves to cases in which $n > 1$. We used a discrete set of values of n, namely the values 1.5, 2.0, 2.5 and 3.0. For each one of these values we scanned the parameter planes described by the Cartesian coordinates (C, π_e), aiming at locating the

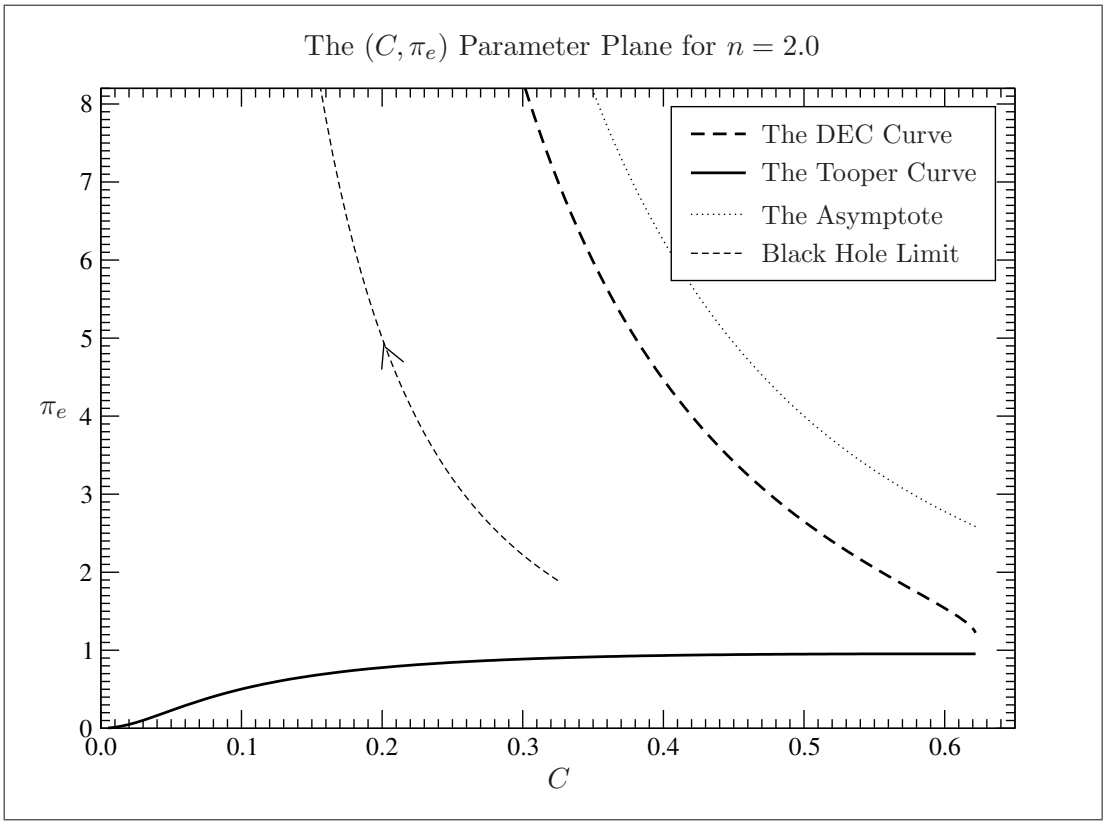

Figure 2: The (C, π_e) parameter plane for the case $n = 2.0$. The Tooper curve approaches the origin as an integer power, namely as C^2. The asymptote is given by $\pi_e = 1/C^{2.0}$.

allowed regions of these parameter planes, that is, the regions where the solutions, first of all exist, and second correspond to physically acceptable matter.

In the Figures from 1 to 4 we present the allowed regions of the parameters planes, for the aforementioned four values of n. As one can see, the four parameter planes shown are generically quite similar. Each point in one of these graphs corresponds to a run of the numerical program with the given values of n, C and π_e, as well as with the value $\xi_e = 1$ for the value of the position of the inflection point of $\gamma(\xi)$, which is the position of the extremum of $\pi(\xi)$, so that $\pi_e = \pi(\xi_e)$. This choice, which since we have that $\xi_e = r_e/r_0$ can be written as $r_e = r_0$, means only that from now on we choose the arbitrary parameter r_0 to be the radial position r_e of this inflection point. The runs were done on a grid with variations of C given by $\Delta C = 0.01$, starting from $C = 0.01$.

Here is the part of the description of the parameter planes which is common to all four cases. The strong solid lines represent the Tooper curves. Over these curves lie the solutions found by Tooper [4] a long time ago. Over these curves we have that $\xi_1 = 0$, meaning that these solution are for filled spheres rather than for shells, and also that $\xi_\mu = 0$, which is the particular condition imposed by Tooper in order to obtain his solutions, which avoids the singularity at the origin. Below these curves there are no acceptable solutions of the differential equation, since the solutions diverge when one integrates towards $\xi = 0$. Later on we will examine in more detail exactly what happens in this case. Therefore, all existing solutions are necessarily above the Tooper curves.

The strong dashed lines represent the Dominant Energy Condition [5] curves (or DEC curves for short). Above these curves the stress-energy tensor of the matter does not satisfy

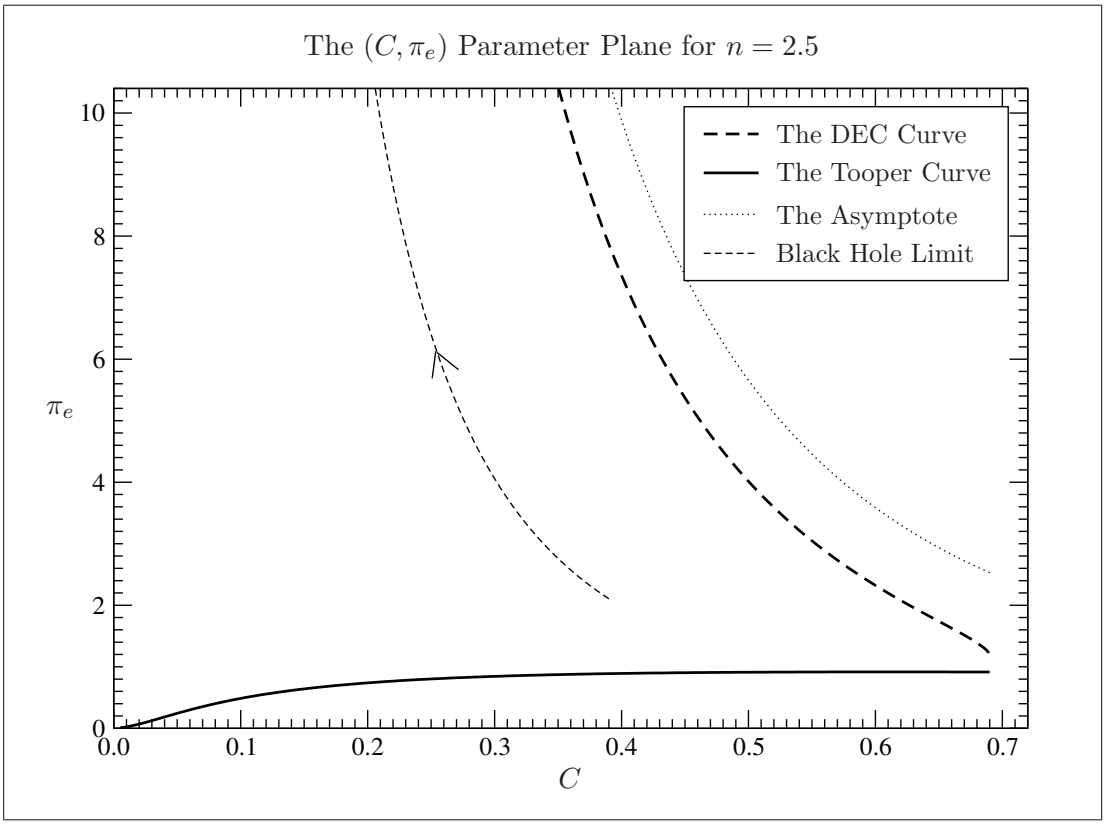

Figure 3: The (C, π_e) parameter plane for the case $n = 2.5$. The Tooper curve approaches the origin as a fractional power, namely as $C^{5/3}$. The asymptote is given by $\pi_e = 1/C^{2.5}$.

this condition, so that the behavior of the matter is not physically acceptable. Note that this does not mean that the solution of the differential equation itself does not exist above these curves, since in general it does in fact exist, and can be calculated without too much trouble. It just means that there is no physically possible matter that would result in these solutions. It can be shown that for very large values of π_e the DEC curves tend asymptotically to the asymptotes shown in the graphs, with the light doted lines, which are given by

$$\pi_e(C) = \frac{1}{C^n}. \tag{28}$$

Note that this implies that the allowed regions extend indefinitely to arbitrarily large values of π_e, always below the DEC curves, and becoming ever closer to $C = 0$. Of course, due to this we can only show a finite portion of these allowed regions in the graphs. Therefore, all physically acceptable solutions are necessarily below the DEC curves, as well as above the Tooper curves. It should be noted that over the $C = 0$ axis there are also no solutions, since in this case, according to the definition of C given immediately after Equation (22), we have that $K = 0$, so that according to the equation of state shown in Equation (8) we then have pressureless dust, and therefore there are no stable static solutions. Therefore all acceptable solutions must have $C > 0$, that is, *strictly* positive C. It should also be noted that, since π_e is the maximum value of the necessarily positive function $\pi(\xi)$, the $\pi_e = 0$ axis corresponds to flat, empty space, since in this case we have that $\pi(\xi) \equiv 0$, which means that $\gamma'(\xi) \equiv 0$ and hence that $\beta'(r) \equiv 0$, which in turn, by Equation (7), implies that $\rho(r) \equiv 0$ and therefore that there is no matter present at all.

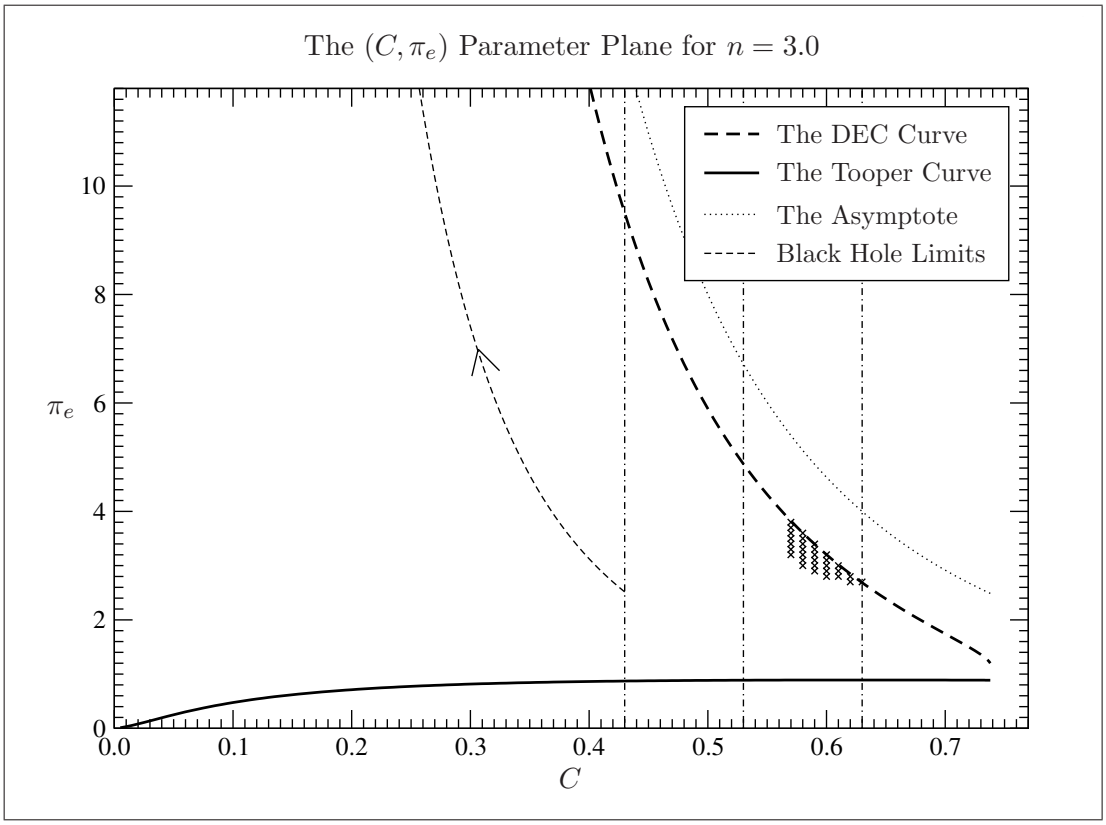

Figure 4: The (C, π_e) parameter plane for the case $n = 3.0$. The Tooper curve approaches the origin as a fractional power, namely as $C^{3/2}$. The asymptote is given by $\pi_e = 1/C^{3.0}$. The vertical lines mark the anomalous region. The crosses mark points where a divergence was detected when integrating outward, towards infinity.

The set of facts just described identifies completely the allowed regions of the solutions, for each value of n. Every solution must be above the Tooper curves, below the DEC curves, and away from the π_e axis. The small remaining gaps between the DEC and Tooper curves, seen on the extreme right of the graphs, are a consequence of the numerical difficulty when running the program in those regions. What seems to happen in this case is that at this point the DEC curves fall off in a very sharp way, and immediately cross the Tooper curves. The effect of this is that, according to the numerical exploration performed so far, there seems to be no acceptable solutions anywhere more than a distance $\Delta C = 0.01$ to the right of these gaps. Therefore, all existing acceptable solutions must also be located to the left of these gaps. Further investigation of these small regions would be numerically expensive, and this seems to be unnecessary at this stage.

In the graphs one can also see the light dashed lines, that represent sequences of allowed solutions that constitute limits that we will describe here as *black hole limits*. What we mean by such a black hole limit is one in which the formation of an event horizon is approached, so that the geometry everywhere outside that horizon tends to be given by the exterior Schwarzschild metric. Note that there is no matter dynamics involved in these limits, they are simply sequences of static solutions. What is being stated here is that there are static solutions, within our family of static solutions, which are as close as one may wish to what is sometimes referred to as a naked black hole solution, at least in what concerns the region strictly outside the event horizon.

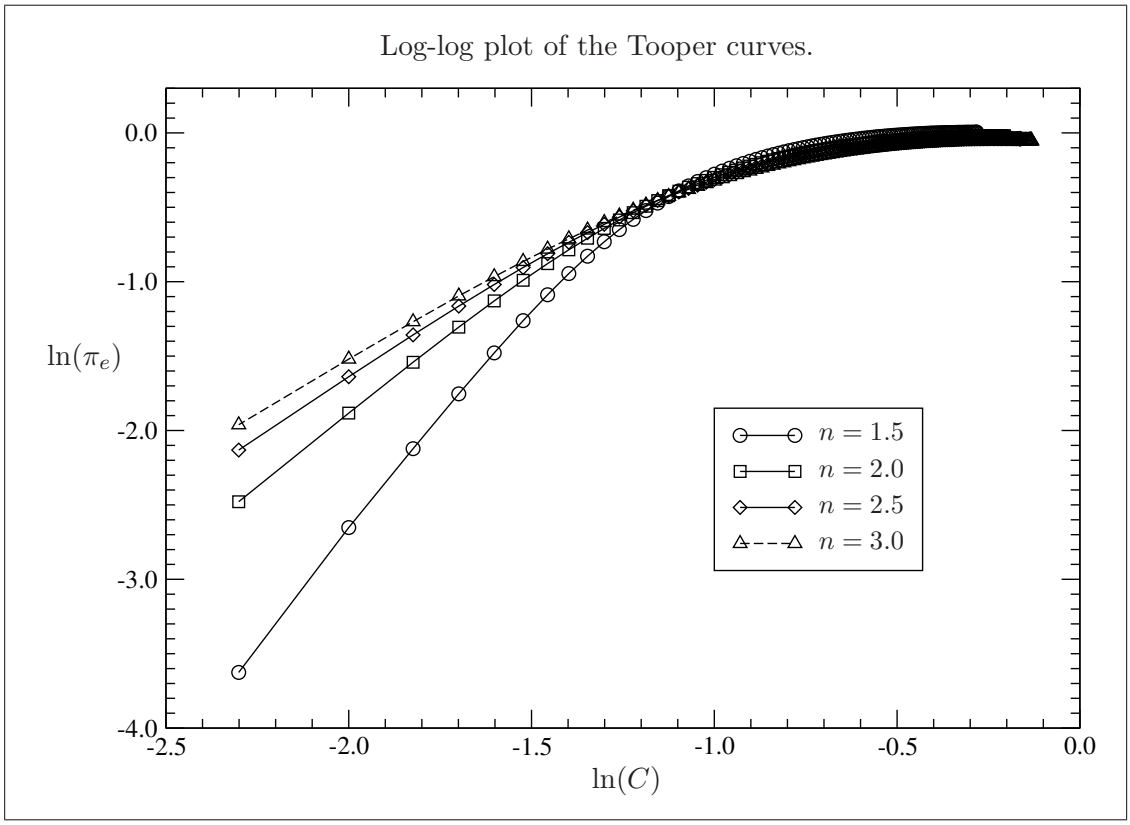

Figure 5: Double logarithmic graph of π_e versus C over the Tooper curves for each value of n, showing that they approach the origin as powers. So long as $n > 1$ the Tooper curves can be written as $\pi_e(C) = \alpha_n C^m$ near the origin, where $m = n/(n-1)$.

We should point out the peculiar behavior of the case $n = 3.0$ for the larger values of C. The vertical lines seen in Figure 4 characterize the region where the behavior is quite different from all other cases. The onset of this anomalous behavior occurs approximately at $C = 0.43$, and is characterized by increasingly larger values of ξ_2 as C is increased, thus leading to long running times for the program, when integrating outward. This behavior becomes severe around $C = 0.53$, with very large values of ξ_2, that can go all the way up to 6×10^4 or more. It seems to cease after $C = 0.63$.

In some cases between $C = 0.53$ and $C = 0.63$ the program even detects a divergence when integrating outward, which is very unusual, and was completely unexpected. This of course represents a failure to satisfy the asymptotic boundary condition, so that in this case the solution does not really exist. The points of the parameter plane where this happens are marked with small crosses in the graph. To the right of $C = 0.63$ the situation seems to normalize to some extent, but still with values of ξ_2 that are significantly larger that usual.

It is uncertain whether these divergent cases are caused by the accumulation of numerical errors during very long integration runs, which could prevent the graph of $\gamma(\xi)$ from crossing the ξ axis. And the opposite effect is also possible, since it is also true that in some cases the graph of $\gamma(\xi)$ may in fact cross the ξ axis *due* to these accumulated numerical errors. The detailed examination of this region would require a large number of very numerically expensive runs, so that for the time being a refinement of this analysis will have to wait.

Note that this anomalous behavior refers only to the outward integration. The integration inward still works in the typical way, even if the outward one diverges. This leads to

partial solutions, which are valid only within finite radial intervals of ξ, from zero to some finite value. They just cannot be extended to radial infinity. These partial solutions may still be relevant, since they may play a role as the inner parts of multi-layered solutions. In this case they do not have to satisfy the asymptotic boundary condition at radial infinity, but rather a set of boundary conditions on an interface located at some finite value of ξ.

Finally, let us point out that the Tooper curves for $n > 1$ all approach the origin $C = 0$ of the graphs behaving like (possibly fractional) powers, as described in the figure captions. In Figure 5 one can see log-log plots of these curves for all values of n that were used. The fact that the left-hand portions of these curves behave like straight lines betrays such a power behavior, so that for each value of n we have that

$$\pi_e(C) \simeq \alpha_n C^m, \tag{29}$$

near to and to the right of the point $C = 0$, where α_n is some constant, and one can abstract from the numerical data that the power m is given by

$$m = \frac{n}{n-1}. \tag{30}$$

Note that this is singular for $n = 1$ and negative for $n < 1$, indicating a profound change in the behavior of the whole system in such cases.

3.1 The Dominant Energy Condition

Since the Dominant Energy Condition (DEC) [5] is a cornerstone of the determination of the allowed regions in the parameters plane of the solution for each value of n, let us derive the form that this condition takes for the polytrope solutions. In order to do this we start with a preliminary discussion of the Weak Energy Condition (WEC) [5]. Let us start, then, by noting that we have for the metric tensor,

$$g_{\mu\nu} = \begin{bmatrix} \mathrm{e}^{2\nu(r)} & 0 & 0 & 0 \\ 0 & -\mathrm{e}^{2\lambda(r)} & 0 & 0 \\ 0 & 0 & -r^2 & 0 \\ 0 & 0 & 0 & -r^2\sin^2(\theta) \end{bmatrix}, \tag{31}$$

and also that we have for the stress-energy tensor,

$$T_{\mu}{}^{\nu} = \begin{bmatrix} \rho(r) & 0 & 0 & 0 \\ 0 & -P(r) & 0 & 0 \\ 0 & 0 & -P(r) & 0 \\ 0 & 0 & 0 & -P(r) \end{bmatrix}. \tag{32}$$

The WEC is a condition on the stress-energy tensor, namely the statement that, for all causal vector fields V^μ, it hold that

$$T_{\mu\nu}V^\mu V^\nu \geq 0. \tag{33}$$

Consider now a completely arbitrary vector field

$$V^\mu = \Big(V_0, V_1, V_2, V_3\Big), \tag{34}$$

so that we get for the corresponding covariant components $V_\mu = g_{\mu\nu}V^\nu$

$$V_\mu = \left(\mathrm{e}^{2\nu(r)} V_0, -\mathrm{e}^{2\lambda(r)} V_1, -r^2 V_2, -r^2 \sin^2(\theta) V_3 \right). \tag{35}$$

This implies that we get for $V^2 = V_\mu V^\mu$

$$V^2 = \mathrm{e}^{2\nu(r)} V_0^2 - \mathrm{e}^{2\lambda(r)} V_1^2 - r^2 V_2^2 - r^2 \sin^2(\theta) V_3^2, \tag{36}$$

on which, for the time being, we will impose no conditions at all. Consider now the vector field W^μ defined by

$$W^\mu = T^\mu{}_\nu V^\nu. \tag{37}$$

In terms of this vector field the tensor expression in the WEC can be written as

$$T^\mu{}_\nu V_\mu V^\nu = V_\mu W^\mu, \tag{38}$$

where

$$W^\mu = \Big(\rho(r) V_0, -P(r) V_1, -P(r) V_2, -P(r) V_3 \Big). \tag{39}$$

Therefore the tensor expression in the WEC, which is the contraction of V^μ and W^μ, reads

$$V_\mu W^\mu = \rho(r)\, \mathrm{e}^{2\nu(r)} V_0^2 + P(r)\, \mathrm{e}^{2\lambda(r)} V_1^2 + P(r) r^2 V_2^2 + P(r) r^2 \sin^2(\theta) V_3^2. \tag{40}$$

Since $\rho(r)$, $P(r)$, the exponentials and the squares are all positive quantities, this is a sum of positive terms, and is therefore positive. We therefore conclude that the WEC is satisfied for all vector fields V^μ, regardless of any conditions imposed on them, and in particular for all causal vector fields, given that from Equations (38) and (40) we have

$$T_\nu{}^\mu V_\mu V^\nu \geq 0, \tag{41}$$

so that the WEC is satisfied. Apparently this is a consequence of the fact that both $g_{\mu\nu}$ and $T_{\mu\nu}$ are diagonal. Since the quantity above is an invariant, this condition of course holds on all reference frames.

Let us now discuss the DEC, which once more is a condition on the stress-energy tensor. Given an arbitrary future-pointing causal vector field V^μ, consider once more the vector field given by $W^\mu = T^\mu{}_\nu V^\nu$. The DEC is the statement that, for all future-pointing causal vector fields V^μ, the vector field W^μ is also a future-pointing causal vector field. Let us consider once more the vector field V^μ and its covariant components V_μ, but we now impose that it is a future-pointing causal vector field, with $V_0 > 0$, and hence that it also satisfy the condition

$$V^2 \geq 0, \tag{42}$$

which from Equation (36) implies that

$$\left[\mathrm{e}^{2\nu(r)} V_0^2 \right] - \left[\mathrm{e}^{2\lambda(r)} V_1^2 + r^2 V_2^2 + r^2 \sin^2(\theta) V_3^2 \right] \geq 0. \tag{43}$$

Let us now consider again the vector field W^μ given in Equation (39), where $W_0 = \rho(r) V_0$ is positive because $\rho(r)$ is positive and because V^μ is a future-pointing causal vector field, so that $V_0 \geq 0$. Let us recall that the DEC consists of the statement that, if V^μ is a future-pointing causal vector field, then W^μ is also a future-pointing causal vector field. Using the metric tensor we have for its covariant components

$$W_\mu = \left(\rho(r)\,\mathrm{e}^{2\nu(r)}V_0, P(r)\,\mathrm{e}^{2\lambda(r)}V_1, P(r)r^2V_2, P(r)r^2\sin^2(\theta)V_3\right). \tag{44}$$

We now simply calculate $W^2 = W_\mu W^\mu$, and thus get

$$\begin{aligned} W^2 &= \rho^2(r)\,\mathrm{e}^{2\nu(r)}V_0^2 - P^2(r)\,\mathrm{e}^{2\lambda(r)}V_1^2 - P^2(r)r^2V_2^2 - P^2(r)r^2\sin^2(\theta)V_3^2 \\ &= \rho^2(r)\left[\mathrm{e}^{2\nu(r)}V_0^2\right] - P^2(r)\left[\mathrm{e}^{2\lambda(r)}V_1^2 + r^2V_2^2 + r^2\sin^2(\theta)V_3^2\right]. \end{aligned} \tag{45}$$

Now, since V^μ is a future-pointing causal vector field we have from Equation (43) the condition for the quantities within brackets in the equation above,

$$\left[\mathrm{e}^{2\nu(r)}V_0^2\right] \geq \left[\mathrm{e}^{2\lambda(r)}V_1^2 + r^2V_2^2 + r^2\sin^2(\theta)V_3^2\right]. \tag{46}$$

Besides, from Equation (45) we have that the condition $W^2 \geq 0$ is equivalent to

$$\rho^2(r)\left[\mathrm{e}^{2\nu(r)}V_0^2\right] \geq P^2(r)\left[\mathrm{e}^{2\lambda(r)}V_1^2 + r^2V_2^2 + r^2\sin^2(\theta)V_3^2\right], \tag{47}$$

and therefore from Equation (46) we conclude that so long as $\rho^2(r) \geq P^2(r)$, and therefore so long as

$$\rho(r) \geq P(r), \tag{48}$$

we have that

$$W^2 \geq 0. \tag{49}$$

Since we also have that $W_0 \geq 0$, it follows that W^μ is a future-pointing causal vector field, so that the DEC is satisfied.

The question then remains of determining when we have the condition $\rho(r) \geq P(r)$ for all values of r within the matter region. Interestingly, it is fairly easy to do this in the case of the solutions for polytropes. If we assume that $\rho(r) \geq P(r)$, which is equivalent to

$$\frac{\bar{P}(r)}{\bar{\rho}(r)} \leq 1, \tag{50}$$

and use the polytropic equation of state in the dimensionless form given in Equation (24), then it follows that

$$\frac{\bar{P}(\xi)}{\bar{\rho}(\xi)} = C\left[\bar{\rho}(\xi)\right]^{1/n}, \tag{51}$$

from which the DEC reduces to

$$C\left[\bar{\rho}(\xi)\right]^{1/n} \leq 1. \tag{52}$$

Recalling from Equation (27) that we have $\bar{\rho}(\xi) = \pi(\xi)/\xi^2$, the condition reduces to

$$\frac{\pi(\xi)}{\xi^2} \leq \frac{1}{C^n}. \tag{53}$$

This must be true for all values of ξ within the matter region. It suffices therefore to impose this condition only at the point where $\bar{\rho}(\xi)$ is maximum, that is, at the point where $\pi(\xi)/\xi^2$ is maximum. However, as one can see in the figures given in [1], for the larger values of π_e, and hence of $\bar{\rho}(\xi)$, the points of maximum of $\bar{\rho}(\xi)$ and of $\pi(\xi)$ tend to coincide, as do the

values of these two quantities at their points of maximum, if we use the value $\xi_e = 1$ for the point of maximum of $\pi(\xi)$, as we do here.

Therefore, if we consider the point $\xi_e = 1$, the position of the inflection point of $\gamma(\xi)$ at which we start the numerical runs, where $\pi(\xi) = \gamma'(\xi)$ has its global maximum π_e, then we see that it is a fair estimate for high-density solutions to consider the DEC curve as located approximately at this point, and thus we arrive at a simple constraint among the free parameters of the solutions, for large values of π_e and $\bar{\rho}(\xi)$,

$$\pi_e \leq \frac{1}{C^n}. \tag{54}$$

This determines the asymptotic behavior of the DEC curve $\pi_e(C)$, for very small values of C and correspondingly very large values of π_e, as shown in the graphs. For each value of the polytropic index n, and given some value of the dimensionless polytropic constant C, the equality case in Equation (53) gives us a maximum allowed value of the parameter π_e. It therefore establishes an allowed region within the (C, π_e) parameter plane of this family of solutions. The exact relation between C and π_e for the DEC curve, given by the equality case in Equation (53), can be easily obtained by numerical means.

3.2 Determination of the DEC Curve

Here we will describe in detail how we determined the position of the DEC curve. For technical reasons, this is better done before the determination of the Tooper curve, as we will see. The program that integrates the differential system given in Equations (21) and (23) has two monitoring procedures installed within it, one for identifying a divergence during the integration, and the other to identify a violation of the DEC. This last one does its job by monitoring the quantities $P(\xi)$ and $\rho(\xi)$ as they are calculated, as well as the ratio $P(\xi)/\rho(\xi)$ of the two, which according to the DEC has to be always below 1. Whenever this ratio goes above 1, at any point ξ, the program creates a flag file to record the event. The existence of this flag file can then be used by another program in order to institute a search for the position of the DEC curve. Note that from Equation (52) the DEC condition can be written as

$$\bar{\rho}(\xi) \leq \frac{1}{C^n}, \tag{55}$$

thus showing that the condition can be written in terms of $\bar{\rho}(\xi)$ only, so that this is the only quantity that we really have to monitor. Starting from the inflection point of $\gamma(\xi)$, as we will always do here, there may be violations of the DEC either when integrating to the right or when integrating to the left. However, in order to search for the position of the DEC curve it suffices to integrate only to the left, due to the following argument. Since from Equation (27) we have that

$$\bar{\rho}(\xi) = \frac{\pi(\xi)}{\xi^2}, \tag{56}$$

and since we will always start the integration from the point of maximum of $\pi(\xi)$, located at $\xi = \xi_e = 1$, taking a derivative with respect to ξ and applying at ξ_e we have that

$$\begin{aligned} \bar{\rho}'(\xi_e) &= \frac{\pi'(\xi_e)}{\xi_e^2} - 2\,\frac{\pi(\xi_e)}{\xi_e^3} \\ &= -2\,\pi(\xi_e), \end{aligned} \tag{57}$$

given that we have that $\pi'(\xi_e) = 0$ and also that $\xi_e = 1$. Since $\pi(\xi_e)$ is a strictly positive quantity, it follows that $\bar{\rho}(\xi)$ increases when we go to the left-hand side of ξ_e and decreases when we go to the right-hand side of it. It follows from this that the point of maximum of $\bar{\rho}(\xi)$ is always located to the left of the point of maximum of $\pi(\xi)$. Therefore, in order to detect a violation of the DEC, it suffices to integrate only to the left of the inflection point.

For each value of n the determination of the DEC curve starts at the lowest value of C for which one wishes to include the DEC curve in the graph. At that point, for that value of C, we start the search at the value of π_e given by the asymptote, which is always above the DEC curve,

$$\pi_e = \frac{1}{C^n}. \tag{58}$$

We then integrate the differential system only to the left, towards the origin, expecting to find a violation of the DEC at this initial point of the search. Once the violation is detected at any point ξ we abort the integration, decrease the value of π_e by a certain variation $\Delta\pi_e$, and repeat the integration. This proceeds until a violation of the DEC is no longer detected, meaning the we are now below the DEC curve. Once this happens we return π_e to its previous value, decrease the variation $\Delta\pi_e$ by some constant factor, and continue the downward search for the position of the DEC curve.

This results in a fast exponential search for the position of the DEC curve, since the variation $\Delta\pi_e$, which represents the distance between the position of the search and the position of the DEC curve, decreases exponentially. Note that we can start with a rather large value of $\Delta\pi_e$, since it will be decreased exponentially fast. We chose to start with $\Delta\pi_e = 0.1$. The stop criterion for this downward search is the condition that the addition of $\Delta\pi_e$ to π_e no longer change π_e, meaning that the relative precision represented by $\Delta\pi_e/\pi_e$ falls below the precision level at which the search program runs. Since that program runs in double precision mode, this guarantees the localization of the DEC curve within that double precision level. Naturally the precision of the results of the search is also affected by the precision with which the differential system is integrated. The integration code runs in quadruple precision mode, and we chose to use an integration interval of $\Delta\xi = 10^{-5}$. Since the integration program uses the Runge-Kutta fourth-order integration algorithm, this results in an excellent level of precision, certainly much greater than what is needed just for the graphs.

Once we have obtained the position of the DEC curve for the current value of C, by means of the inner loop over values of π_e, we enter an outer loop in which we now change the values of C. We increment C by a fixed variation ΔC, which will characterize the grid size used for the graphs. We chose to use $\Delta C = 0.01$. Having the new value of C, we repeat the whole search process downward, for the position of the DEC curve. In this next search process we use as the initial value of π_e the last value of this variable obtained in the previous search process. Due to the properties of the DEC curve, which has negative derivative everywhere, this starting value of π_e is guaranteed to be above the DEC curve at the new value of C, but it is much closer to it than an initial value based on the asymptote, thus making the search more efficient.

The stop criterion for the loop over values of C is that, when the current exponential search downward over π_e concludes, the integration program detect, in its last run, the presence of a divergence. This detection will also result in the creation of a flag file recording the event, to be used by external programs. The presence of a divergence means that the downward search over π_e not only found the DEC curve, but also crossed below the Tooper curve at that value of C. Once the DEC curve has either been crossed or has become

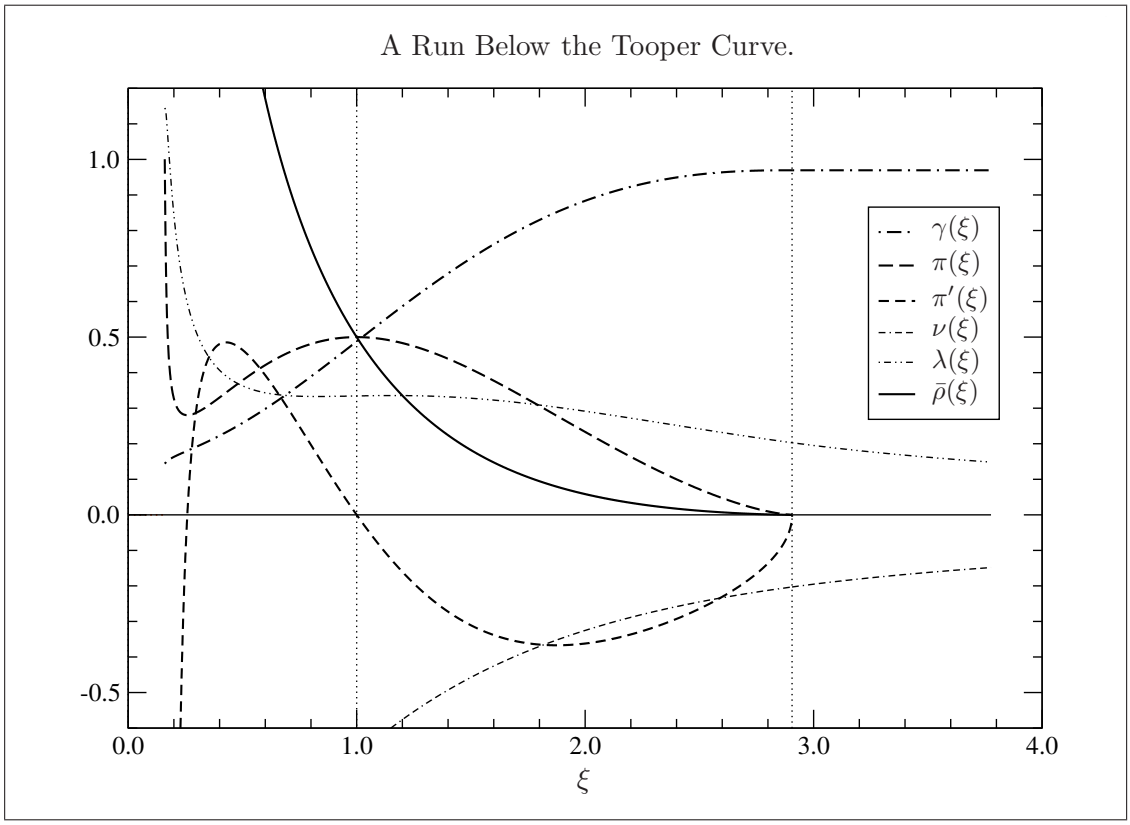

Figure 6: All the functions obtained from a trial solution of the differential equation with parameters below the Tooper curve. The integration diverges when one integrates towards the origin. The left vertical line marks the initial point of the integration to either side, and the right vertical line marks the position of ξ_2 as obtained by the integration to the right side. The parameters used were $n = 1.5$, $C = 1/3$, $\xi_e = 1.0$ and $\pi_e = 0.5$.

sufficiently close to the Tooper curve, there is no longer any chance of finding any point (C, π_e) of the parameter plane that is both below the DEC curve and above the Tooper curve, within the precision limitations with which the graphs are being produced.

3.3 Determination of the Tooper Curve

The determination of the position of the Tooper curve relies on the detection of divergences in the integration process, when one crosses below that curve. We should therefore examine in more detail, before anything else, what happens when we try to run the program below the curve. The program would usually stop cold when a divergence is detected, but there is an option to still run it for a little while, in order to plot the graph shown in Figure 6, where one can see a representation of the behavior of the differential system when we run below the Tooper curve, in a simple case, with the parameters $n = 1.5$, $C = 1/3$ and $\pi_e = 0.5$. The behavior shown is quite typical. The graph shows all the relevant quantities as functions of the radial variable ξ. The left vertical dotted line, located at $\xi = 1$, is the location at which we start the integration of the differential equation shown in Equation (21), to either side. The integration to the right-hand side proceeds normally and produces a value $\xi_2 \approx 2.9$ for the outer radius, as indicated by the right vertical dotted line. To the right of this point we have the exterior Schwarzschild solution, with $\xi_M \approx 0.97$.

However, the integration to the left-hand side cannot be completed, a value for ξ_1 is

never found, and the process has to be interrupted when divergences are detected. As one can see in Figure 6, the function $\gamma(\xi)$ never crosses the ξ axis, and never develops a constant value around the origin. Its derivative $\pi(\xi)$ does not assume a second zero, and instead turns around and diverges quickly to positive infinity. The second derivative $\pi'(\xi)$ diverges even faster to negative infinity. The graphs of the metric functions $\lambda(\xi)$ and $\nu(\xi)$ do not cross one another, and in fact diverge to positive and negative infinity respectively, which is the exact opposite of their usual behavior, when the two graphs do cross, and then diverge in the opposite directions. The dimensionless matter energy density $\bar{\rho}(\xi)$ displays a strong divergence to infinity, and therefore so does $\rho(\xi)$, thus characterizing a hard singularity of the matter energy density.

In this simple case it can be determined that the derivative $\pi(\xi)$ diverges to infinity faster than $1/\xi$, and therefore that neither $\pi(\xi)$ nor $\bar{\rho}(\xi)$ are integrable functions around the origin. However, due to the singular behavior of the measure factor $\exp[\lambda(\xi) + \nu(\xi)]$ near the origin, it is unclear whether or not this divergence corresponds to a either a finite or an infinite total amount of energy around the origin. The detection of the divergence included in the integration program consists of detecting the turnaround of the function $\pi(\xi)$, and therefore the change of sign of its derivative $\pi'(\xi)$.

Let us now describe in detail how we determined the position of the Tooper curve. This was done once the DEC curve had already been determined. The exponential search downward towards the Tooper curve proceeded exactly like that for the DEC curve. For each value of n the determination of the Tooper curve starts at the largest value of C for which the position of the DEC curve was successfully determined. At that point, for that value of C, we start the downward search at the value of π_e given by the DEC curve, which is always above the Tooper curve. Since we are looking for a divergence when integrating inward, we integrate the differential system to the left only, towards the origin. If the integration concludes with no divergence, resulting therefore in a definite value for ξ_1, we decrease the value of π_e by a certain variation $\Delta\pi_e$, and repeat the integration. This proceeds until a divergence is detected, meaning that we are now below the Tooper curve. Once this happens we abort the integration, return π_e to its previous value, decreases the variation $\Delta\pi_e$ by some constant factor, and continues the downward search for the position of the Tooper curve.

Once again this results in a fast exponential search, this time for the position of the Tooper curve, since the variation $\Delta\pi_e$, which represents the distance between the position of the search and the position of the Tooper curve, decreases exponentially. Note once again that we can start with a rather large value of $\Delta\pi_e$, since it will be decreased exponentially fast, and again we chose to start with $\Delta\pi_e = 0.1$. Once more the stop criterion for this downward search is the condition that the addition of $\Delta\pi_e$ to π_e no longer change π_e, meaning that the relative precision represented by $\Delta\pi_e/\pi_e$ falls below the precision level at which the search program runs. Since this second search program also runs in double precision mode, this guarantees the localization of the Tooper curve within that double precision level. Naturally, once again the precision of the results of the search is also affected by the precision with which the differential system is integrated. We recall that the integration code runs in quadruple precision mode, and again we chose to use an integration interval of $\Delta\xi = 10^{-5}$. Since the integration program uses the Runge-Kutta fourth-order integration algorithm, once again this results in an excellent level of precision, certainly much greater than what is needed just for the graphs.

Once we have obtained the position of the Tooper curve for the current value of C, by means of the inner loop over values of π_e, we enter an outer loop in which we now change the values of C, which we will now decrease rather than increase. We decrease C by a fixed

variation ΔC, which will characterize the grid size used for the graphs. Again we chose to use $\Delta C = 0.01$. Having the new value of C, we repeat the whole search process downward, for the position of the Tooper curve. In this next search process we use as the initial value of π_e the last value of this variable obtained in the previous search process. Due to the properties of the Tooper curve, which has positive derivative everywhere, this starting value of π_e is guaranteed to be above the Tooper curve at the new value of C, but it is much closer to it than an initial value based on the DEC curve, again making the search more efficient. The stop criterion for the loop over values of C is that C would become zero or negative at the next decrement. This can be done by checking whether the current value of C is such that $C \leq \Delta C$. We therefore stop the process of determining the Tooper curve at $C = \Delta C$.

It should be noted that the stop criterion for the loop over π_e may fail in some cases, if we are very close to $C = 0$. This is so because, specially for the case $n = 1.5$, the Tooper curve approaches $C = 0$ with zero derivative. This tends to make π_e and $\Delta\pi_e$ always commensurate in this case, so that the test that the addition of $\Delta\pi_e$ to π_e fails to change π_e may never succeed. Due to this it was necessary to implement a maximum number of iterations of the loop over π_e, which we chose to be 52. The average number of iterations in order to locate the Tooper curve within the double precision level is a little over 32.

3.4 Alternative for the Tooper Solutions

Since in our current system of dimensionless variables the determination of the solution exactly over the Tooper curve is somewhat tricky, given the instability due to the fact that the program will fail rather catastrophically even an infinitesimal mount below that curve, it is worth mentioning that there is an alternative way to obtain the solutions in this case. As we approach the Tooper curve in the parameter plane the point of maximum of the dimensionless energy density $\bar{\rho}(\xi)$ migrates to the origin $\xi = 0$. In the limit, when we hit the Tooper curve, it has a certain maximum value $\bar{\rho}_0$ located at that origin, where we also have that $\bar{\rho}'(0) = 0$. Since according to Equation (56) we have that

$$\pi(\xi) = \xi^2 \bar{\rho}(\xi), \tag{59}$$

it follows that $\pi(\xi)$ behaves as $\bar{\rho}_0 \xi^2$ near the origin, and hence that $\gamma(\xi)$ behaves as $(\bar{\rho}_0/3)\,\xi^3$ there. Since both the function $\gamma(\xi)$ and its derivative $\pi(\xi)$, as well as the second derivative $\pi'(\xi)$, all start at zero at $\xi = 0$, it is clear that we cannot use these variables in order to integrate the equation starting from the origin. However, we can rewrite our equations in terms of the function $\bar{\rho}(\xi)$ instead of $\pi(\xi)$, and this will allow us to integrate the differential system from the origin, since we have that $\bar{\rho}(0) = \bar{\rho}_0 \neq 0$. If we do this we obtain the following pair of coupled ordinary differential equations,

$$\bar{\rho}'(\xi) = -\bar{\rho}(\xi)\,\frac{n}{n+1}\,\frac{1}{\xi - \gamma(\xi)}\,\frac{1+F(\bar{\rho})}{2F(\bar{\rho})}\left[\frac{\gamma(\xi)}{\xi} + F(\bar{\rho})\xi^2\bar{\rho}(\xi)\right], \tag{60}$$

$$\gamma'(\xi) = \xi^2\bar{\rho}(\xi), \tag{61}$$

where

$$F(\bar{\rho}) = C[\bar{\rho}(\xi)]^{1/n}. \tag{62}$$

This first-order differential system determines the two variables $\gamma(\xi)$ and $\bar{\rho}(\xi)$ in terms of ξ, with the initial conditions $\gamma(0) = 0$ and $\bar{\rho}(0) = \bar{\rho}_0$ at the origin $\xi = 0$. Once $\bar{\rho}(\xi)$ is determined, we can also determine $\pi(\xi)$ using Equation (59). Note that we have here only

three free parameters, namely n, C and $\bar{\rho}_0$, where this last one will determine both ξ_2 and ξ_M, as well as ξ_e. On the other hand, ξ_1 and ξ_μ are fixed at zero. Since we are now constrained to be over the one-dimensional Tooper curve, we have one less free parameter as compared to the constraint of being within the two-dimensional allowed region of the parameter plane. Using this alternative method one can get the Tooper solutions more easily, and this is in fact essentially what Tooper did in [4].

4 Mapping the Observables

On a second phase of the exploration we measured certain observables over the allowed regions, in order to characterize the general behavior of the solutions throughout the regions. These can be considered as diagnostic observables, and they can be seen in Figures from 7 to 10. Using them we may, for example, classify the solutions as corresponding to either low-density or high-density distributions of matter, or as being either close to or distant from forming an event horizon.

Each run of the program produces four fundamental numbers as results that characterize that solution, given by the dimensionfull radii r_1, r_μ, r_2 and r_M, and hence by the corresponding dimensionless quantities ξ_1, ξ_μ, ξ_2 and ξ_M. These are all encoded in the function $\gamma(\xi)$; ξ_μ is the constant value of $\gamma(\xi)$ within the inner vacuum region, that is, to the left of ξ_1; ξ_1 is the point where $\pi(\xi) = \gamma'(\xi)$ becomes zero when integrating inwards; ξ_M is the constant value of $\gamma(\xi)$ within the outer vacuum region, that is, to the right of ξ_2; ξ_2 is the point where $\pi(\xi) = \gamma'(\xi)$ becomes zero when integrating outwards.

All these quantities have well-defined physical meanings, although we believe that in the case of r_μ the complete physical meaning has not yet been completely established; r_1 is the inner radius, or the radial coordinate characterizing the inner vacuum region; r_μ, at least for the time being, has only the meaning of being zero for the Tooper solutions; r_2 is the outer radius, or the radial coordinate characterizing the overall size of the matter distribution; r_M is the Schwarzschild radius, associated to the total mass M and to the total energy Mc^2 of the bound gravitational system. Next we will define our diagnostic observables and describe their main properties.

4.1 Definition of the Observables

We will define, for the purposes of the calculations with the program, three ratios involving the quantities ξ_1, ξ_μ, ξ_2 and ξ_M, that will have useful properties regarding the characterization of the solutions. All these ratios will assume values within the interval $[0, 1]$. The first one we will name the *Energy Ratio*, which is defined as

$$\begin{aligned} E_R &= \frac{r_\mu}{r_M + r_\mu} \\ &= \frac{\xi_\mu}{\xi_M + \xi_\mu}. \end{aligned} \tag{63}$$

This quantity has the property that it is zero when $\xi_\mu = 0$, and hence it characterizes the Tooper curve in this way. It also has the property that if ξ_μ is very large, with $\xi_\mu \gg \xi_M$, then it approaches the value 1. This $E_R \to 1$ limit characterizes, therefore, solutions which are *maximally different* from the Tooper solutions. Presumably these are solutions in which other forms of energy are more important than the energy associated to the total asymptotic gravitational mass M.

The second ratio we will name the *Horizon Ratio*, defined as

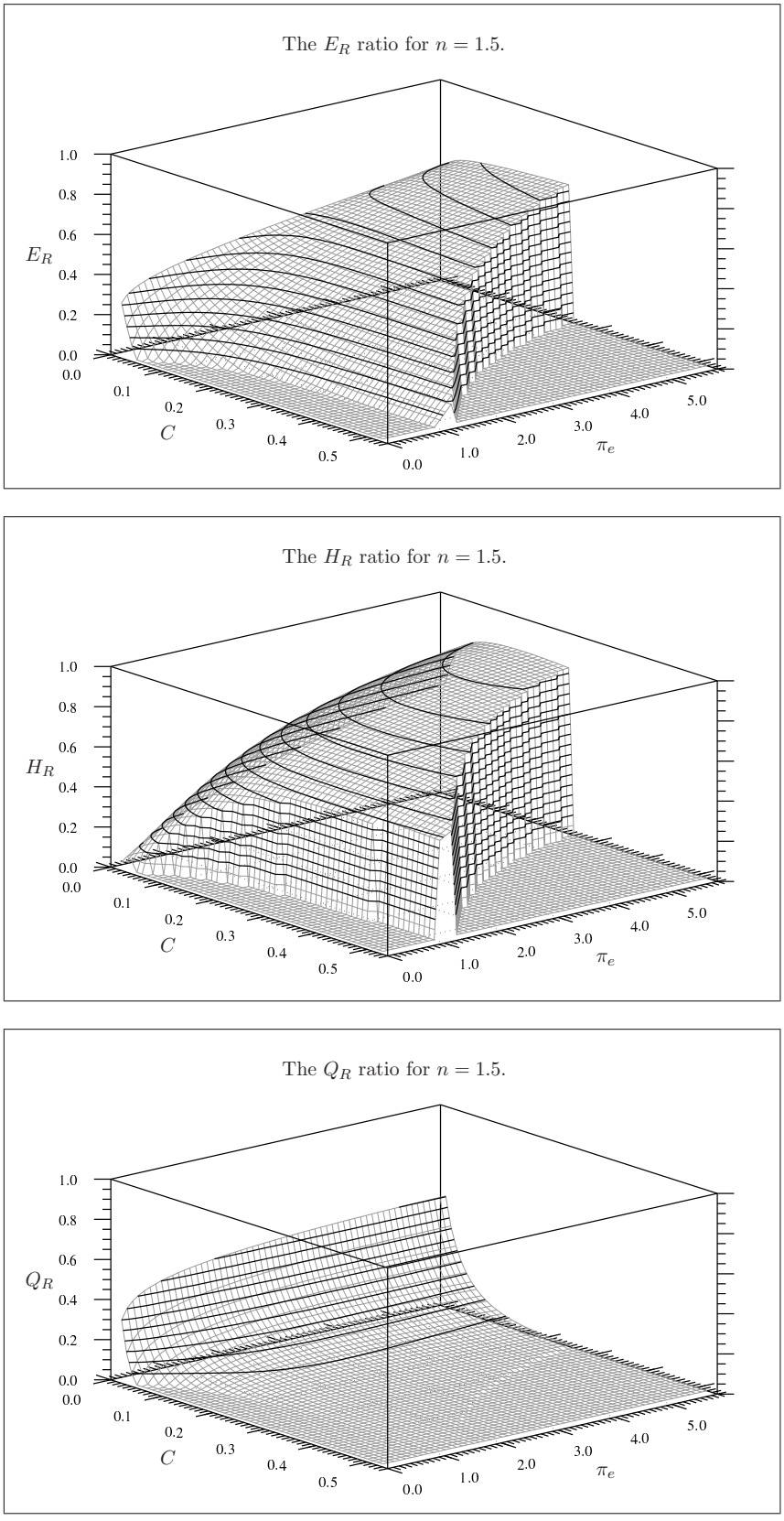

Figure 7: The observables energy ratio E_R, horizon ratio H_R and quantum ratio Q_R for $n = 1.5$. The contour curves are spaced vertically by 0.05.

$$H_R = \frac{r_M}{r_2} = \frac{\xi_M}{\xi_2}. \tag{64}$$

Since all our solutions here have the property that $\xi_M < \xi_2$, this quantity is always smaller than 1. However, there may be limits in which it approaches 1. This quantity has the property that for very low-density objects, for which $\xi_M \ll \xi_2$, is approaches zero. Therefore, this observable indicates low-density solutions when it is small, as is the case over the Tooper curves for small values of C. On the other hand, if ξ_M and ξ_2 become very close, then this ratio approaches 1. In this case one approaches a situation in which an event horizon forms at the position ξ_2, according to the exterior Schwarzschild solution, which is valid outside ξ_2, and which in this case acquires the well-known coordinate singularity at ξ_2. Therefore this ratio discriminates between low-density and high-density solutions, including the onset of black hole solutions, in the $H_R \to 1$ limit.

The third ratio we will name the *Quantum Ratio*, defined as

$$Q_R = \frac{r_1}{r_2} = \frac{\xi_1}{\xi_2}. \tag{65}$$

Clearly the name chosen requires some explanation. This has the property that it is zero if $\xi_1 = 0$, in which case we have solutions for filled spheres, instead of shells. In this way, it characterizes the Tooper curve just like E_R, but since there are many other solutions for which $\xi_1 \ll \xi_2$, even if $\xi_1 \neq 0$, this diagnostic is not particularly helpful.

On the other hand, if we recall that all the matter in the system is located between ξ_1 and ξ_2, we see that when the inner radius approaches the outer radius the proper volume containing the matter shrinks to zero, resulting in infinite localized matter densities. If we consider the radial coordinate, we have that in this case the coordinate thickness $\xi_2 - \xi_1$ of the shell goes to zero, so that the corresponding proper length will eventually become commensurate with the correlation lengths (or wavelengths) of the fields associated to the particles of matter within the shell. In this case it is to be expected that the quantum behavior of the matter will prevent this thickness from decreasing any further. In other words, it is reasonable to expect that the quantum properties of the matter will prevent the shell from degenerating into a true two-dimensional surface. Therefore, the limit $Q_R \to 1$ indicates situations in which the quantum properties of matter come into play.

4.2 Behavior of the Observables

As one can see in the graphs shown in Figures from 7 to 10, the qualitative behavior of the ratios E_R, H_R and Q_R as functions of C and π_e is quite similar for all the values of n explored, thus indicating that the same is at least qualitatively true for ξ_1, ξ_μ, ξ_2 and ξ_M as well. In all graphs there are essentially the same regions with the same specific properties for the solutions, with the possible exception of the rather small anomalous region for the larger values of C, in the case $n = 3.0$.

Let us start by describing how each one of the three ratios behaves along the allowed regions. The ratio E_R goes to zero at the Tooper curves, as expected, thus pinpointing the locations of these curves. It seems to increase towards 1 as we enter the asymptotic parts of the allowed regions, with $C \to 0$ and $\pi_e \to \infty$, thus indicating that ξ_μ becomes very large as we travel deeper into these regions.

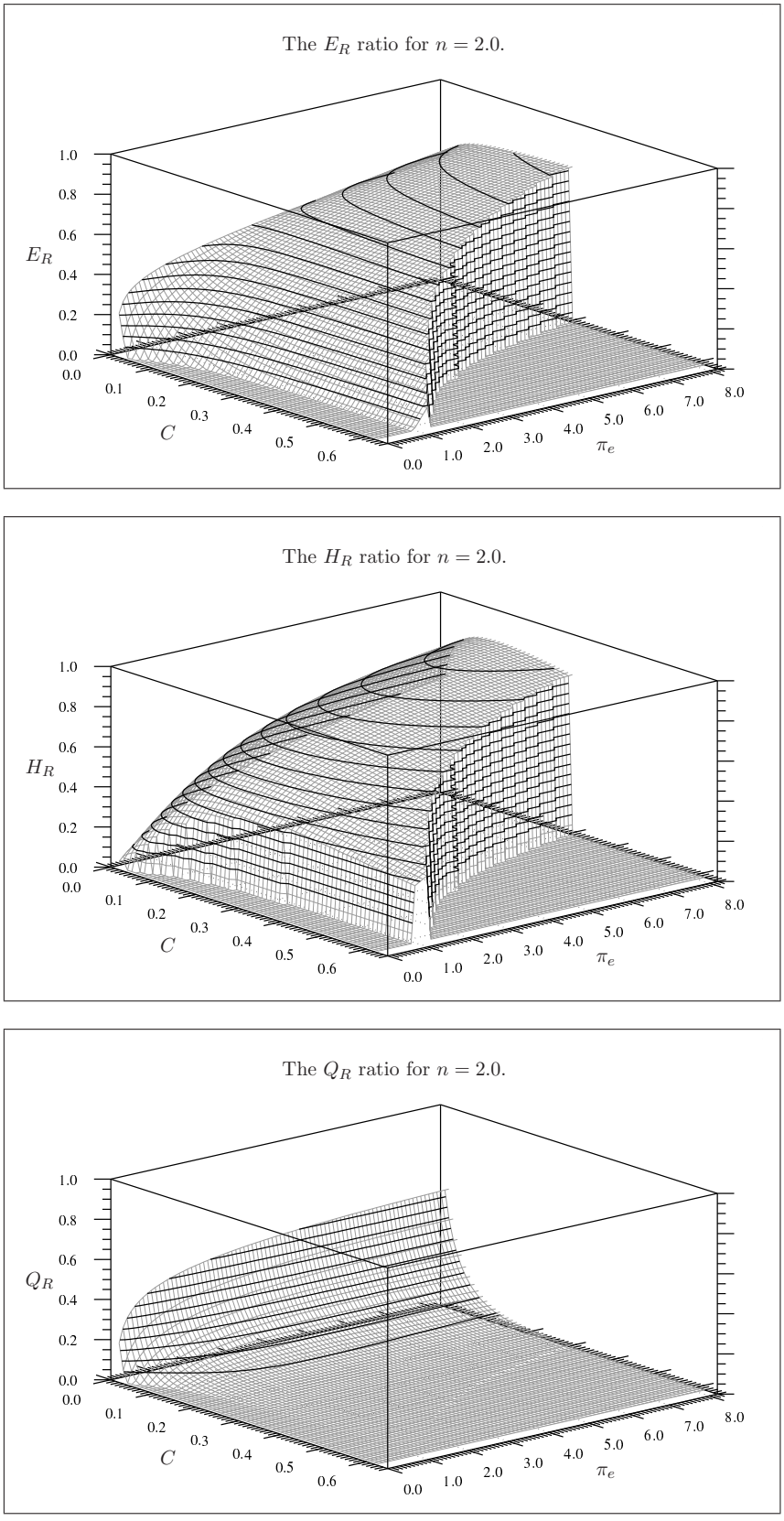

Figure 8: The observables energy ratio E_R, horizon ratio H_R and quantum ratio Q_R for $n = 2.0$. The contour curves are spaced vertically by 0.05.

The ratio H_R has values smaller than 1, but sometimes not close to zero, over the whole length of the Tooper curves, and very small values near the point $C = 0$. This means that there may be solutions with significant overall matter density on the Tooper curve, specially in the case $N = 1.5$. There are also solutions with very small such density near $C = 0$. This ratio also seems to increase towards 1 as we enter the asymptotic parts of the allowed regions, with $C \to 0$ and $\pi_e \to \infty$, thus indicating that as we travel deeper into these regions we proceed towards high overall densities and the formation of event horizons.

The ratio Q_R is zero over the whole length of the Tooper curves, thus indicating that we have $\xi_1 = 0$ there, as expected. It is also either zero or very small over most of the allowed regions, thus indicating that in general we have $\xi_1 \ll \xi_2$. It only becomes significantly larger than zero for small C, near the π_e axis. Also, it can be seen that it increases slowly as we travel into the asymptotic regions. This indicates that on limits for which $C \to 0$ and $\pi_e \to \infty$ within these regions the quantum effect on the matter will eventually come into play.

Examining what happens in each part of the allowed regions, some general conclusions can be formulated. To begin with, over or near the Tooper curves we never have the formation of event horizons. The same is true for the parts of the DEC curves shown in the graphs. Another way to say this is to point out that for finite and non-zero values of C the solutions also never form horizons, and that for the larger values of C they never get anywhere even close to that.

For each value of n the asymptotic region, where $C \to 0$ and $\pi_e \to \infty$, is the one region where we can approach the formation of an event horizon. This is also the region where we get extremely high overall matter densities, since this density increases as we enter more deeply into this asymptotic region. The exploration of the black hole limits in these asymptotic regions would require a whole new set of runs, and will have to be postponed to a future paper.

The two basic properties of the Tooper curves, that over them we have $\xi_1 = 0$ and $\xi_\mu = 0$, are confirmed by our exploration. Very low density objects seem to exist mostly near the origin, for very small values of both C and π_e. That seems to be the realm of the main-sequence stars. It may be possible to find somewhat similar solutions in the small mostly regular region located beyond the anomalous region of the case $n = 3.0$, but at this point it is not really clear what the true character of these solutions may be.

Below the Tooper curves, that is for very small values of π_e, given certain values of n and C, as well as for sufficiently large C, there are no solutions at all. The upper limit for C is somewhere between 0.5 and 0.8 depending on the value of n. As a curious point of some interest here, let us point out that the case in which we have $n \to \infty$ and $C = 1/3$ corresponds to a gas of photons, or of some other type of massless particles, for which we do not expect to find any static solutions.

Close to the DEC curve we have extremely relativistic matter, with overall matter densities that vary from significant to very high. Presumably in this case the speed of sound in the gas is close to the speed of light, and it is possible that the average speed of thermal agitation is also close to the speed of light. This implies immense thermal energies and temperatures, and it can be imagined that this also helps to prevents the formation of event horizons. Anyway, these cases seem to be far beyond any objects that one could hope to find in nature.

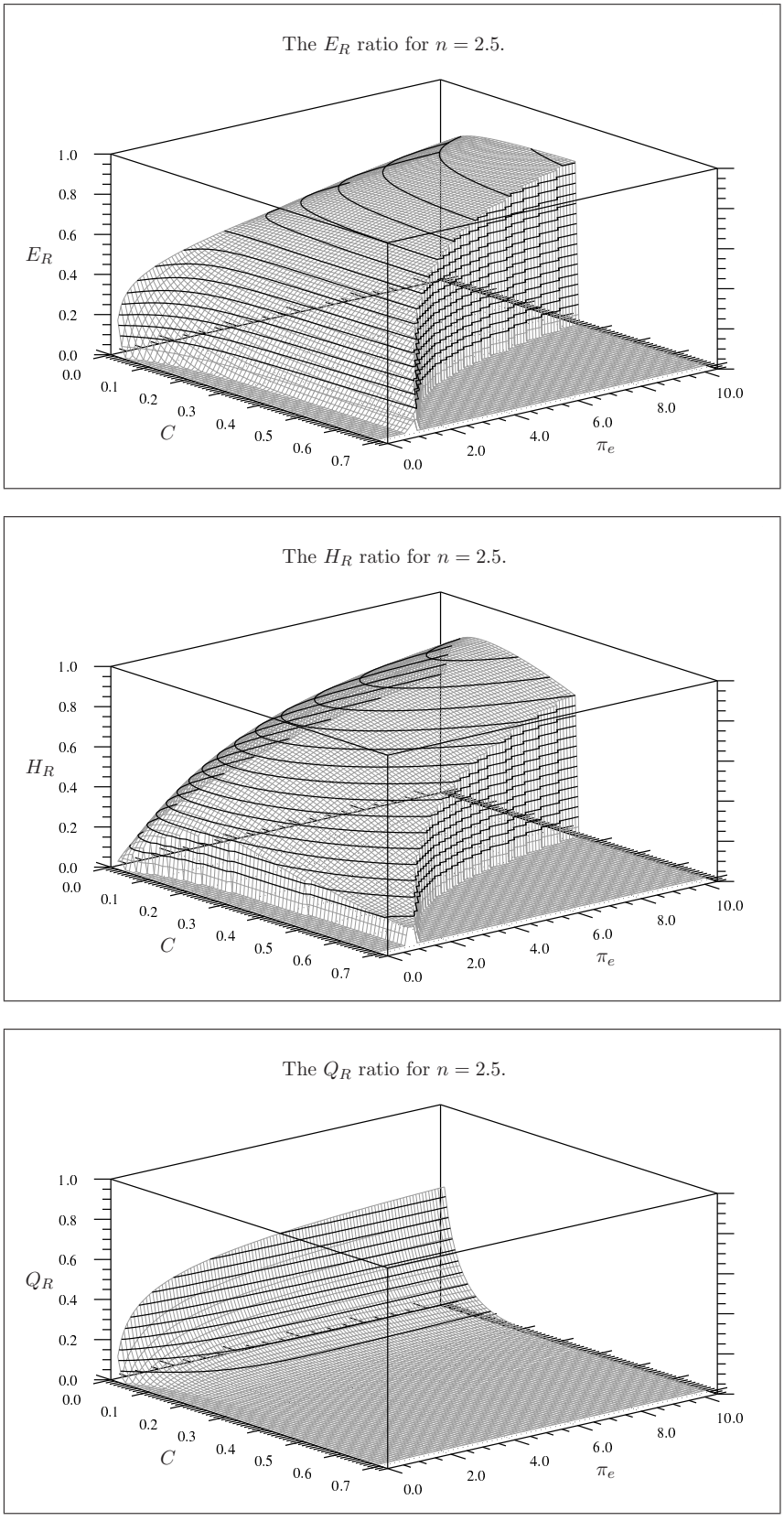

Figure 9: The observables energy ratio E_R, horizon ratio H_R and quantum ratio Q_R for $n = 2.5$. The contour curves are spaced vertically by 0.05.

5 Application to Astrophysics

Let us now discuss how one can use this family of solutions in order to obtain the solutions for definite objects, say with given mass and outer radius. To start with, let us assume that we want the solution for an object of mass M, and therefore with Schwarzschild radius r_M. The problem poses itself of what values of n, C and π_e should be used in order to obtain a solution with the required properties. Note that the value of M is not directly involved in the choice of these dimensionless parameters. There is no single solution to this first problem, but rather a significant amount of free choice involved.

Regarding the value of n, one can either choose an appropriate value of n to represent the type of behavior of the matter involved, or one can construct, for example, a two-layer solution, with layers that are connected by means of appropriate interface boundary conditions at a certain interface between two different layers of matter, with different thermodynamic behaviors. A two-layer model of a star with a radiative inner layer, say with $n = 3.0$, and an isentropic outer layer, say with $n = 1.5$, comes to mind. Putting aside for now this more complex alternatives, let us just assume that we simply chose some value of n for a single-layer solution.

For any values of C and π_e that one chooses to run the program with, assuming that the point (C, π_e) is within the allowed region of the parameter plane for the value of n to be used, there will result definite values for ξ_1, ξ_μ, ξ_2 and ξ_M. If we have a required value of r_M, then we can at once determine the parameter r_0, for any values of C and π_e whatsoever, since we have that

$$r_0 = \frac{r_M}{\xi_M}. \tag{66}$$

This determines the position r_0 of the inflection points of both $\beta(r)$ and $\gamma(\xi)$, and therefore the position of the point of maximum of $\pi(\xi)$. Having determined r_0, we can now determine all other relevant dimensionfull quantities, since we have that

$$r_1 = \xi_1 r_0, \tag{67}$$

$$r_\mu = \xi_\mu r_0, \tag{68}$$

$$r_2 = \xi_2 r_0. \tag{69}$$

We therefore see that there are solution for all possible positive values of r_M, and hence of M. The fact that the parameter r_M was factored out of the system, when we wrote it in terms of dimensionless parameters, betrays the existence of a scaling transformation among the solutions, parametrized by the value of r_M. Any point (C, π_e) of the parameter plane corresponds in fact to an infinite set of similar solutions, for all possible values of r_M, and hence of M. At this point we may also determine the polytropic constant K, since we have that

$$K = C\left(\kappa r_0^2\right)^{1/n}, \tag{70}$$

where $\kappa = 8\pi G/c^4$. If one wants to have a certain given value, say, for r_2, then it will be necessary to explore the parameter plane in order to find a point (C, π_e) that yields the required values of both M and r_2. And again there may be more than just one such point.

Note that, given n, since we still have the two free parameters C and π_e, we have open to us the possibility of choosing freely one more property of the object under study, besides the mass and the outer radius, and still have the means to find the corresponding solutions. For example, we may require that $r_\mu = 0$, which will put us squarely on top of the Tooper

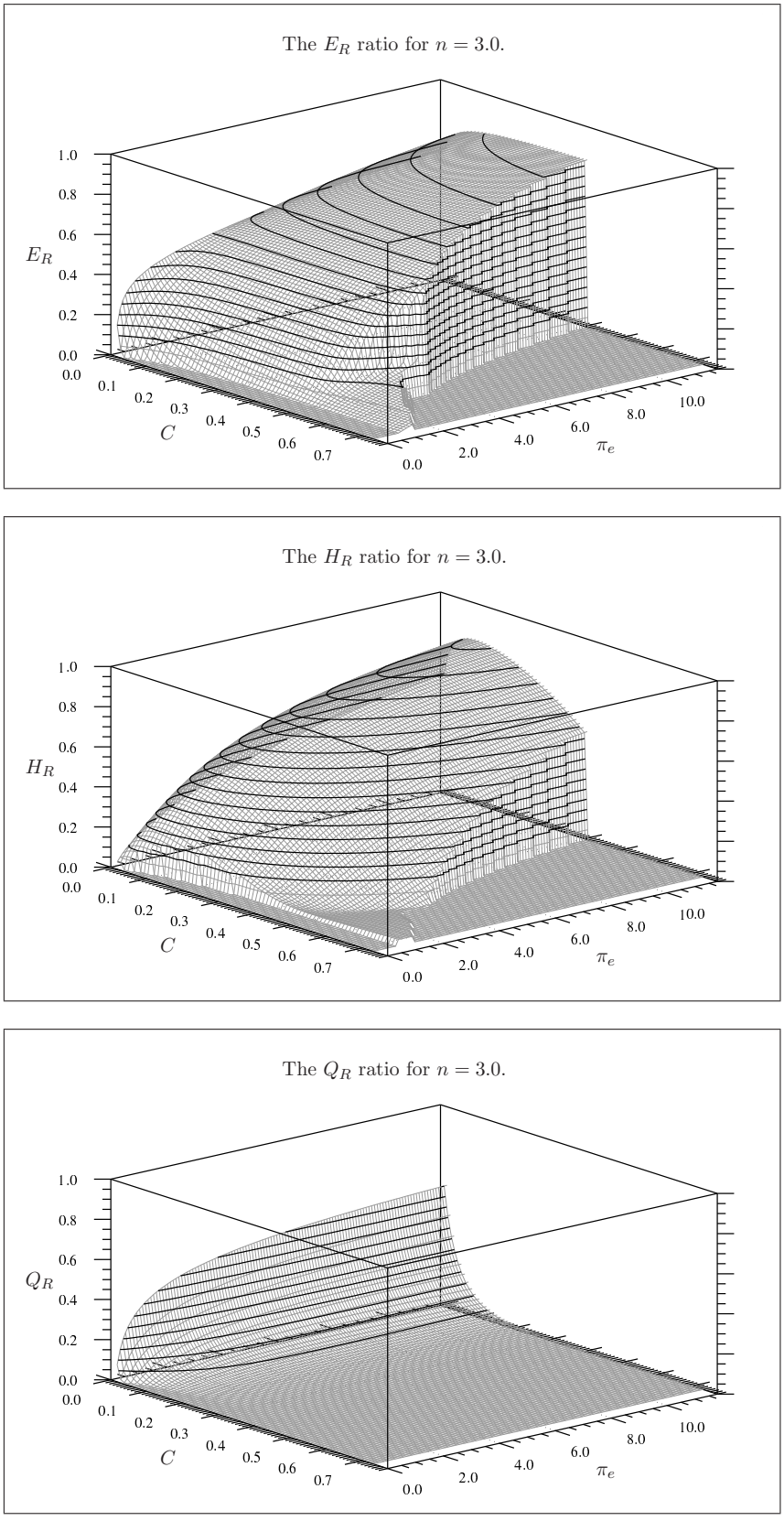

Figure 10: The observables energy ratio E_R, horizon ratio H_R and quantum ratio Q_R for $n = 3.0$. The contour curves are spaced vertically by 0.05.

curve. But a more interesting alternative does immediately come to mind, that of choosing the surface temperature of the object. If and when this was done, it could result in a complete map of the relations between mass, outer radius and surface temperature of stars, which might even be verifiable against observations. However, that would require a detailed and fully relativistic study of the temperature and hence of the energy in the context of these solutions, which we are currently not prepared to deliver. And of course it would probably be far more compelling to do this in the context of a two-layer model for the stars.

Given the way in which one has to use the program in order to obtain solutions with specific given properties, it would be useful to have approximate numerical functions implementing either $(\xi_1, \xi_\mu, \xi_2, \xi_M)$ or (r_1, r_μ, r_2, r_M) in terms of n, C and π_e. These could then be used to solve numerically for the parameters needed in order to obtain, for example, some required mass and outer radius. Even the function data generated in order to produce the graphs shown in Figures from 7 to 10, or the graphs themselves, could, at least in principle, be used for that purpose. For example, if one requires M to be, say, the mass of the Sun, and r_2 to be its outer radius, this determines the value of the ratio $H_R(C, \pi_e) = r_M/r_2$, which in turn determines a curve on the (C, π_e) parameter plane. Running the program at any point on this curve will generate a solution for the required values of M and r_2. This means, of course, that we are still able to require some given value for one more characteristic of the Sun, such as its surface temperature.

6 Conclusions

Unlike the Schwarzschild, Reissner-Nordström and Kerr-Newman solutions of the Einstein field equations, which represent static vacua and are valid only in the exterior region of a spherically or axially symmetric material object, the family of solutions for polytropic matter that we presented in [1] consists of static and spherically symmetric solutions valid over the whole extend of the three-dimensional manifold. This makes them of particular interest as models for astrophysical objects, in both the low-density case, such as main sequence stars, and in the high-density case, particularly in the case of black holes or objects close to them in terms of their exterior metric structure.

In the previous paper [1], in which the solutions were presented, we also presented a few examples of such solutions, both with low and high matter densities, including both the functions that represent the matter and the functions that represent the geometry. However, even in its dimensionless form, this is a rather large three-parameter set of solutions, and of course due to space limitations we could give only a few illustrative examples. In this paper we explored a significant part of this three-dimensional parameter space, in order to establish both the existence of specific solutions and some of the main properties of these solutions.

We did this for a small set of values of the polytropic index n that includes some of those which are most often used in astrophysics. These are usually either integer of half-integer, but it should be pointed out that neither the solutions nor the program have any limitations regarding the use of real numbers for n, other than that n must be strictly positive and finite. The other free dimensionless parameters of the family of solutions are the dimensionless polytropic constant C and the maximum value π_e of the necessarily positive function $\pi(\xi)$, which is the derivative of the function $\gamma(\xi)$, which in turn is the central element of the whole family of solutions.

The existence of the solutions hinges on the existence of the radial positions r_1 and r_2, that is, on the existence of values of r at which the matter energy density $\rho(r)$ becomes

exactly zero. These are also the positions ξ_1 and ξ_2 where the derivative $\pi(\xi)$ of the function $\gamma(\xi)$ becomes exactly zero. We found that many such solutions do in fact exist, in various different regions of the (C, π_e) parameter planes, for each value of n that was tried. These solutions span a large space of possibilities, from very low-density solutions to very high-density ones. Also, it seems that there exist solutions that are as close as one may wish to situations in which an event horizon exists, but this sector requires further exploration.

Besides examining the question of the existence of the solutions, we also examined the behavior of the matter using the Dominant Energy Condition (DEC). This condition determines whether or not the matter associated to the solutions behaves in a physically acceptable way. We found that there are many solutions for which this condition is satisfied. Combining the condition of existence and the DEC we located the allowed regions of the parameter planes, where all physically acceptable solutions are located. These regions have asymptotic sub-regions, for very large values of π_e, in which we are led to surmise that solutions representing black holes, or solutions in some sense close to them, are located.

Of course these asymptotic regions will have to be explored using approaches other than mapping the complete regions, and thus such an effort will have to be postponed to a future paper. Besides these asymptotic regions, there are other small regions which might deserve further scrutiny, as was pointed out in the text. And we should not forget that the cases with $n < 1$, which promise to be significantly different from the ones explores here, are still to be examined in any amount of detail.

However, we would like to finish by pointing out that the most significant limitation of this set of solutions is a rather fundamental one, namely that they do not include the angular momentum of rotating objects. The extension of these solutions to that case remains as a very significant and important open challenge.

Acknowledgments

The author would like to thank Mr. Rodrigo de A. Orselli and Prof. C. E. I. Carneiro for all their help during the work that eventually led to this paper, as well as for their reading of the manuscript and helpful criticism regarding this work.

Data Availability Statement

Data sharing not applicable to this article as no datasets were generated or analyzed during the current study.

References

[1] J. L. deLyra and C. E. I. Carneiro, "Complete solution of the einstein field equations for a spherical distribution of polytropic matter," 2021. DOI: 10.5281/zenodo.5087722.

[2] J. L. deLyra, R. de A. Orselli, and C. E. I. Carneiro, "Exact solution of the einstein field equations for a spherical shell of fluid matter," *arXiv*, vol. gr-qc/2101.02012, 2021. DOI: 10.5281/zenodo.5087611.

[3] P. A. M. Dirac, *General Theory of Relativity*. John Wiley & Sons, Inc., 1975. ISBN 0-471-21575-9.

[4] R. F. Tooper, "General relativistic polytropic fluid spheres," *Astrophys. J.*, vol. 140, pp. 434–459, 1964.

[5] R. Wald, *General Relativity*. University of Chicago Press, 2010.